IEICE Electronics Express, Vol.* No.*,*-*

Broadband Asymmetric Transmission of Linear Polarization in a Tri-layer Chiral Metasurface

Hailin Cao[1-2a)], Xiaodong Wu[1], Junpeng Liu[1], Dian Li[1], Xiaoheng Tan[1], Jianmei Lei[3], Xianhua Han[4]

[1]*Laboratory of Aerocraft Tracking, Telemetering & Command and Communication (Ministry of Education), Chongqing University, 400044 Chongqing, China*

[2]*State Key Laboratory of Power Transmission Equipment & System Security and New Technology, Chongqing University, 400044 Chongqing, China*

[3]*National Motor Vehicle Quality Supervision and inspection Center, China Automotive Engineering Research Institute Co., Ltd, 401122 Chongqing, China*

[4]*The Artificial Intelligence Research Center, National Institute of Adavance Industrial Science and Technology, 2-3-26, Aomi, Koto-ku, Tokyo 135-0064, Japan*

a) hailincao@cqu.edu.cn

Abstract: In this paper, we report a novel tri-layer structure consisting of diamond-shaped metallic strips sandwiched between two sub-wavelength gratings arrays and printed on two dielectric substrates with a broadband asymmetric transmission phenomenon. Due to the Fabry-Pérot-like effect, the cross-polarization conversion can reach a maximum of 0.94 and exceed 0.7 from 10 GHz to 30 GHz exhibiting a broadband characteristic in microwave spectra. Moreover, our structure is compactness both in the propagating direction and in the transverse directions. It is hoped that the proposed simple, easily fabricated chiral metasurface can be used in further polarization conversion devices and nonreciprocal EM devices.

Keywords: Asymmetry transmission, Fabry-Pérot-like effect, cross polarization conversion

Classification: Microwave and millimeter wave devices, circuits, and systems

References

[1] H. L. Cao, *et al.*: "Dual-band polarization conversion based on non-twisted Q-shaped metasurface," Opt. Commun. **370** (2016) 311 (DOI: 10.1016/j.optcom.2016.03.036).

[2] H. L. Cao, *et al.*: "Compact e-shape metasurface with dual-band circular polarization conversion," Opt. Commun. **381** (2016) 48 (DOI: 10.1016/j.optcom.2016.06.046).

[3] H. L. Cao, *et al.*: "Dual-band polarization angle independent 90 °polarization rotator using chiral metamaterial," IEICE Electron. Express **13** (2016) 48 (DOI: 10.1587/elex.13.20160583).

[4] V. A. Fedotov, *et al.*: "Asymmetric Propagation of Electromagnetic Waves through a Planar Chiral Structure," Phys. Rev. Lett. **97** (2006) 167401 (DOI: 10.1103/PhysRevLett.97.167401).

[5] R. Singh, *et al.*: "Asymmetric Propagation of Electromagnetic Waves through a Planar Chiral Structure," Phys. Rev. B **80** (2009) 153104 (DOI: 10.1103/PhysRevLett.97.167401).

[6] Z. M. Zhou, H. L. Yang: "Asymmetric Propagation of Electromagnetic Waves through a Planar Chiral Structure," Appl. Phys. A. **119** (2015) 115 (DOI: 10.1103/PhysRevLett.97.167401).

[7] E. Plum, *et al.*: "Extrinsic electromagnetic chirality in metamaterials," J. Opt. A: Pure Appl. Opt. **11** (2009) 074009 (DOI: 10.1088/1464-4258/11/7/074009).

[8] E. Plum, *et al.*: "Planar metamaterial with transmission and reflection that depend on the direction of incidence," Appl. Phys. Lett. **94** (2009) 131901 (DOI: 10.1063/1.3109780).

[9] M. Kang, *et al.*: "Asymmetric transmission for linearly polarized electromagnetic radiation," Opt. Express **19** (2011) 8347 (DOI: 10.1364/OE.19.008347).

[10] M. Mutlu, *et al.*: "Asymmetric transmission of linearly polarized waves and polarization angle dependent wave rotation using a chiral metamaterial," Opt. Express **19** (2011) 14290 (DOI: 10.1364/OE.19.014290).

[11] M. Mutlu, *et al.*: "Diodelike Asymmetric Transmission of Linearly Polarized Waves Using Magnetoelectric Coupling and Electromagnetic Wave Tunneling," Phys. Rev. Lett. **108** (2012) 213905 (DOI: 10.1103/PhysRevLett.108.213905).

[12] R. Singh, *et al.*: "Terahertz metamaterial with asymmetric transmission," Phys. Rev. B **80** (2009) 153104 (DOI: 10.1103/PhysRevB.80.153104).

[13] L. Chen, *et al.*: "Observation of electromagnetically induced transparency-like transmission in terahertz asymmetric waveguide-cavities systems," Opt. Lett. **38** (2008) 1379 (DOI: 10.1364/OL.38.001379).

[14] V. A. Fedotov, *et al.*: "Asymmetric Transmission of Light and Enantiomerically merically Sensitive Plasmon Resonance in Planar Chiral Nanostructures," Nano Lett. **7** (2007) 1996 (DOI: 10.1021/nl0707961).

[15] A. S. Schwanecke, *et al.*: "Nanostructured Metal Film with Asymmetric Optical Transmission," Nano letters, **8** (2008) 2940 (DOI: 10.1021/nl801794d).

[16] C. Menzel, *et al.*: "Asymmetric Transmission of Linearly Polarized Light at Optical Metamaterials," Phys. Rev. Lett. **104** (2010) 253902 (DOI: 10.1103/PhysRevLett.104.253902).

[17] C. Huang, *et al.*: "Asymmetric electromagnetic wave transmission of linear polarization via polarization conversion through chiral metamaterial structures," Phys.Rev. B **85** (2012) 195131 (DOI:10.1103/PhysRevB.85.195131).

[18] Y. Cheng, *et al.*: "An ultrathin transparent metamaterial polarization transformer based on a twist-split-ring resonator," Appl. Phys. A **111** (2013)

209 (DOI: 10.1007/s00339-013-7546-1).

[19] J. H. Shi, *et al.*: "Tunable symmetric and asymmetric resonances in an asymmetrical split-ring metamaterial," J. Appl. Phys. **112** (2012) 073522 (DOI: 10.1063/1.4757961).

[20] M. Kang, *et al.*: "Asymmetric transmission for linearly polarized electromagnetic radiation," Opt. Express **19** (2011) 8347 (DOI: 10.1364/OE.19.008347).

[21] M. Stolarek, *et al.*: "Asymmetric transmission of terahertz radiationthrough a double grating," Opt. Lett. **38** (2013) 839 (DOI: 10.1364/OL.38.000839).

[22] M. Mutlu, *et al.*: "Asymmetric transmission of linearly polarized waves and polarization angle dependent wave rotation using a chiral metamaterial," Opt. Express **19** (2011) 14290 (DOI: 10.1364/OE.19.014290).

[23] J. Shi, *et al.*: "Dual-band asymmetric transmission of linear polarization in bilayered chiral metamaterial," Appl. Phys. Lett. **102** (2013) 191905 (DOI: 10.1063/1.4805075).

[24] Z. Wei, *et al.*: "Broadband polarization transformation via enhanced asymmetric transmission through arrays of twisted complementary split-ring resonators," Appl. Phys. Lett. **99** (2011) 221907 (DOI: 10.1063/1.3664774).

[25] D. Y. Liu, *et al.*: "Enhanced asymmetric transmission due to Fabry-Perot-like cavity," Opt. Express **22** (2014) 11707 (DOI: 10.1364/OE.22.011707).

[26] K. Song, *et al.*: "High-efficiency broadband and multiband cross-polarization conversion using chiral metamaterial ," J. Phys. D: Appl. Phys. **47** (2014) 505104 (DOI: 10.1088/0022-3727/47/50/505104).

[27] D. Y. Liu, *et al.*: "Diode-like asymmetric transmission of circularly polarized waves," Appl. Phys. A **116** (2014) 9 (DOI: 10.1007/s00339-014-8519-8).

[28] Z. Y. Xiao, *et al.*: "Multi-band transmissions of chiral metamaterials based on Fabry-Perot like resonators," Opt. Express **23** (2015) 7053 (DOI: 10.1364/OE.23.007053).

[29] K. K. Xu, *et al.*: "Ultra-broad band and dual-band highly efficient polarization conversion based on the three-layered chiral structure," Physica E: Low-dimens.Syst. Nanostruct. **81** (2016) 169 (DOI: 10.1016/j.physe.2016.03.015).

[30] K. K. Xu, *et al.*: "Dual-band asymmetric transmission of both linearly and circularly polarized waves based on chiral meta-surface," Opt. Quant. Electron. **48** (2016) 381 (10.1007/s11082-016-0646-3).

[31] D. J. Liu, *et al.*: "Broadband asymmetric transmission and multi-band 90^{o} polarization rotator of linearly polarized wave based on multi-layered metamaterial," Opt. Commun. **354** (2015) 272 (DOI: 10.1016/j.optcom.2015.04.043).

1 Introduction

Metamaterials have recently attracted a tremendous amount of attention due to their intriguing properties, e.g., negative refraction, optical activity and circular dichroism [1-3]. Another remarkable effect is the asymmetric transmission (AT) phenomenon first observed by Fedotov *et al* [4]. The phenomenon of AT resembles the non-reciprocal Faraday effect in magnetized media but takes place in the absence of any magnetic field [5]. The AT effect is defined as the difference in total cross-polarized transmission between the forward and backward

propagating EM waves. It can be well explained by the de Hoop reciprocity as revealed by the Jones matrix formulation [6]. This effect can be used to design polarization conversion devices and nonreciprocal EM devices, which play a fundamental role in many fields, including spectroscopy, optical engineering and the biosciences.

Many structures based on chiral metamaterials (CMMs) have been reported to achieve asymmetric transmission for linear and circular polarized waves ranging across the microwave [7-11], terahertz [12-13], and optical spectra [14-16]. In the early study of the AT effect, the proposed devices based on bi-layer planar structures only operated in a narrow frequency range and had a low magnitude, which seriously restricted their applications. For example, in 2010, Menzel *et al* [16] reported a bi-layer chiral structure that achieved a magnitude of only 0.25 for a linearly polarized wave. Subsequently, many researchers [10, 17-22] proposed a lot of structures to achieve the AT effect phenomenon for linearly polarized waves, but the magnitude of the AT effects was no greater than 0.8. After that, Shi *et al* [23] designed a bilayer chiral metamaterial that can efficiently achieve a maximum magnitude greater than 0.93, but a conspicuous shortcoming is that this strong AT effect can only be observed at a specific resonant frequency.

The growing interests in the AT effect using artificial chiral media are driven by the desire to create metamaterials with a broad operating band and high magnitude. Many recent studies have used the multi-layer structure instead of a coupling bi-layer one to achieve the AT effect with the broad bandwidth and high-magnitude transmission coefficients. It has been confirmed that this intriguing features benefit from the Fabry-Pérot-like mechanism effect, thereby intensely enhancing the transmission efficiency and widen the operating frequency band of the structure. Wei *et al* [24] initially proposed a CMM consisting of arrays of twisted complementary split-ring resonators. Subsequently, Liu *et al* [25] reported a three-layer CMM structure that consists of a ring-chain structure sandwiched between two orthogonal cut-wire arrays and their dielectric layers. This structure can achieve the cross-polarization transmission coefficients T_{xy} greater than 0.5, while T_{yy} are no greater than 0.05 from 2.7 to 14.3 GHz. To the author's knowledge, this is the first time that the broadband AT effect has been achieved using the Fabry-Pérot-like mechanism in the microwave frequency range. A variety of the structures taking advantage of the Fabry-Pérot-like mechanism have been proposed [26-29] in the microwave and even in the THz region [30-31].

In this paper, we propose and study a novel tri-layer chiral metasurface that consists of two grating arrays and diamond-shaped metallic strips forming two isolated Fabry-Pérot-like cavities. Relative to the previous multi-layer structures that are sandwiched by split-ring resonators [28, 29, 31] or ring-chain resonators [27], we point out that the tri-layer structure sandwiched by the diamond resonators exhibits more desirable EM properties. Both simulated and experimental results show that our structure can manipulate the EM waves in a broad band from 10 to 30 GHz (nearly 20 GHz) with a high-magnitude AT effect. It also has the excellent transmission characteristic of flatter tops in the pass band and greater out-of-band rejection. These properties have not been observed in

previous studies. Moreover, our structure have an obvious improvement in the compactness of the geometry with respect to that of previous excellent works both in the propagating direction and in the transverse directions ($\lambda/4.13\times\lambda/4.13\times\lambda/9.4$). Considering these properties, we believe that our proposed structure will enrich the designing application of electromagnetic devices, such as polarization conversion devices and nonreciprocal EM devices.

2 Simulation and experiments setup

Fig. 1 shows the schematic of one periodic unit cell of the designed CMM, which consists of tri-layer metal plates patterned on three sides of two substrates. The pattern of the bottom grating is in an orthogonal form of the upper one, and the middle layer is diamond-shaped metallic strips. The geometric parameters for the unit cell are as follows: L=5 mm, d=1.1 mm, W1=0.5 mm, W2=0.5 mm, a=3.262 mm and θ=135°. The substrate is an FR-4 board with the dielectric constant of 4.3 and loss tangent of 0.025. The copper layers on each sides of the substrate are 35-μm thick.

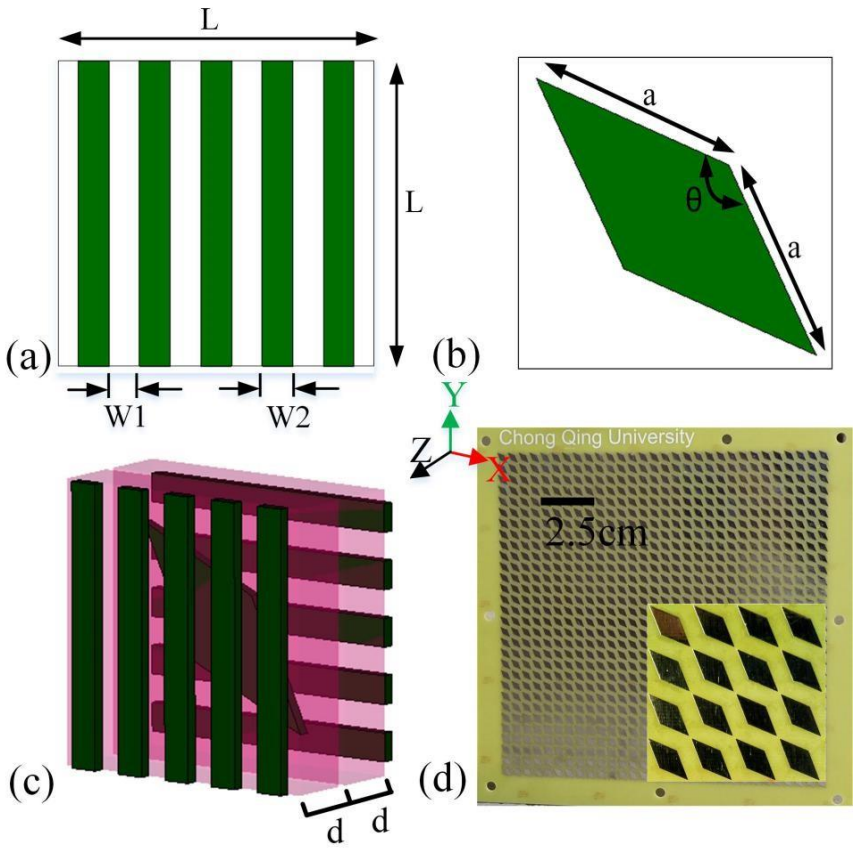

Fig. 1. Schematic of the unit cell of the proposed structure. (a) Top metallic layer and (b) middle metallic layer. (c) Perspective view of the designed unit cell. (d) Photograph of the middle side of a fabricated sample.

We start the analysis with numerical simulations of the CMM structure using CST Microwave Studio. The boundaries are selected to be periodic in the x and y

directions and open in the z direction. The structure is assumed to be periodic and infinite in the x and y directions. Two orthogonal linearly polarized incident waves were used for excitation.

For the experiments, we fabricated a sample of the proposed model with PCB technology; a photograph of the structure is shown in Fig. 1(d). The structure has the dimensions of 30 by 30 unit cells. The experimental measurement is conducted by using two standard broadband double-ridged horn antennas (ETS Model 3116C). The fabricated prototype is fixed in the middle position between the transmitting antenna and the receiving antenna. Next, a vector network analyzer (Agilent E8363C) is used to acquire the transmission coefficients. For the experiments, transmission characteristics of this structure were measured in a microwave anechoic chamber to avoid unwanted reflections.

3 Analysis and Results

3.1. AT effect of the designed tri-layer structure

Fig. 2 shows the simulated and experimental results for the transmission matrix elements of the designed structure for propagation in the backward (-z) and forward (+z) directions. And the experimental results are in good agreement with the simulation ones, except for a slight shift. These undesired discrepancies primarily arise due to fabrication errors in the experiments.

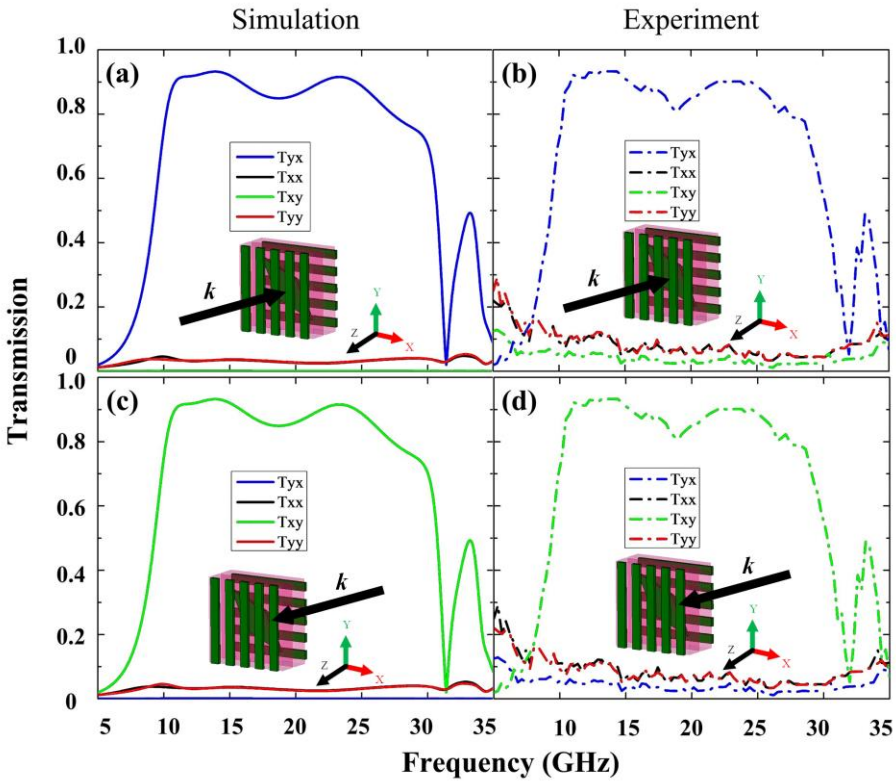

Fig. 2. Simulated and experimental results of transmission coefficient for linearly polarized wave propagation in backward -z (a), (b) and forward +z (c), (d) directions, respectively.

Fig. 2(a) and (b) show the simulated and experimental results for the

backward (-z) propagating incident waves. And Fig. 2(c) and (d) show the simulated and experimental results for the forward (+z) propagating incident waves. In Fig. 2(a) the cross-polarized transmission coefficients T_{yx} are larger than 0.7 from 10 to 30 GHz, while co-polarized transmission coefficients T_{xx} are no greater than 0.05 across the whole frequency. And T_{yx} reach two resonant peaks of 0.94 and 0.92 at 13.6 and 23.4 GHz, respectively. So the incident x-polarized waves almost completely convert into the y-polarized waves. However, the y-polarized incident waves can only reach a maximum of 0.05 in the frequency band of interest, whether for the cross-polarized transmission or co-polarized transmission. When the incident direction is reversed, i.e., in the forward direction as shown in Fig. 2(c), the transmission matrix components of T_{xy} and T_{yx} interchange with each other corresponding to the backward direction, so only the y-polarized incident waves can efficiently convert to the x-polarized waves in the forward propagating direction.

The AT effects are usually characterized by the parameter Δ, which can be used to represent the difference between the transmissions of two opposite propagation directions. For the linear polarization case, the asymmetric transmission parameter Δ can be expressed as follows [17]:

$$\Delta_{lin}^{x} = |T_{yx}^{b}|^2 - |T_{yx}^{f}|^2 \tag{1}$$

$$\Delta_{lin}^{y} = |T_{xy}^{b}|^2 - |T_{xy}^{f}|^2 \tag{2}$$

$$|T_{yx}^{f}| = |T_{xy}^{b}|, \quad |T_{xy}^{f}| = |T_{yx}^{b}| \tag{3}$$

$$\Delta_{lin}^{x} = -\Delta_{lin}^{y} \tag{4}$$

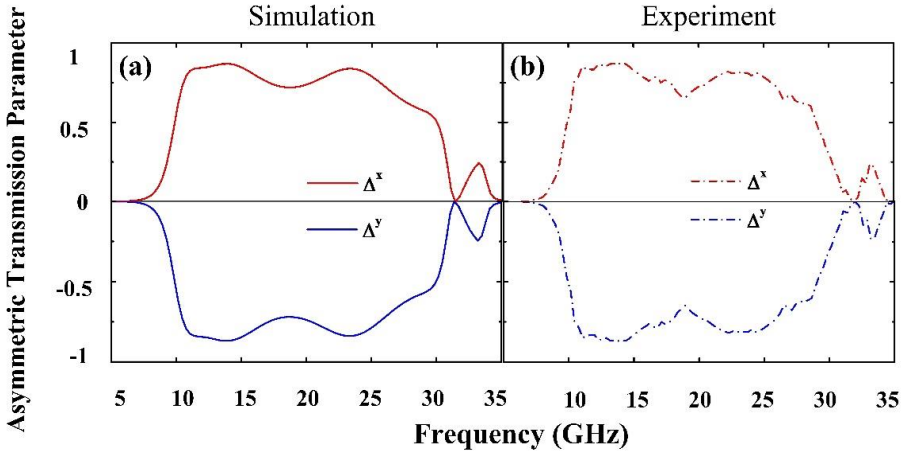

Fig. 3. (a) Simulated and (b) experimental results of AT parameters Δ for our proposed structure

The asymmetric transmission parameter Δ is calculated using Eq. (1)-(2) for the linear polarization waves, and the results are illustrated in Fig. 3. When increasing the frequency, the value of Δ for linear polarization experiences an increase and reaches maxima of 0.86 and 0.84 at frequencies of 13.6 and 23.4 GHz, respectively. Moreover, it has excellent characteristics with flatter tops in the pass band and greater out-of-band rejection. And the curve of Δ^x is exactly the minus

curve of Δ^y for linear polarization, which can be well explained by Eq. (3)-(4).

3.2. Mechanism of broad operating band and high magnitude property

The enhanced cross-polarization conversion phenomenon results from the Fabry-Pérot-like cavity formed by the dielectric substrate separated by the three layers of metasurface. As illustrated in Fig. 4, the x-polarized incident waves convert into the y-polarized waves by incessant decomposition and combination when the traveling waves meet the discontinuous medium material. To further analyze the mechanism of the broad operating band and high magnitude property of this structure, we study the transmission coefficients of the single-layer B, bi-layer BC, and three-layer ABC, respectively. It is noted that in the following analysis we only consider the case that the incident waves transmit through the slab in the backward direction.

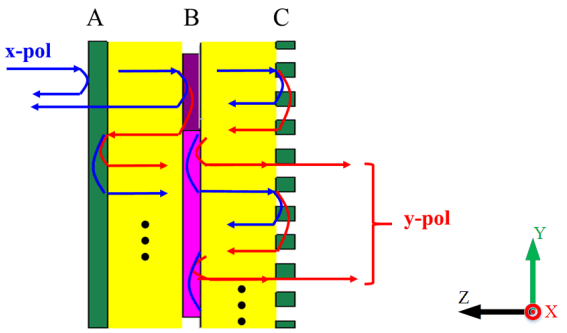

Fig. 4. Schematic graph of Fabry-Pérot-like mechanism model (side view of the three-layer ABC)

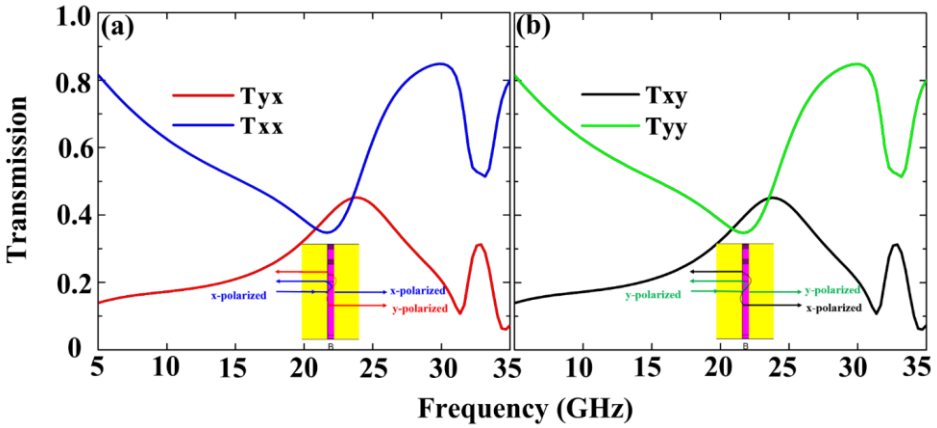

Fig. 5. Transmission coefficients of (a) x-polarized incident wave and (b) y-polarized incident wave: schematic graph of Fabry-Pérot-like mechanism model (side view of single-layer B).

First, considering the condition of only layer B, we simulate both the x-polarized and y-polarized incident wave transmission coefficients. As shown in Fig. 5, the magnitudes of the cross-polarization and co-polarization transmissions are the same owing to the symmetry plane that is 45 °inclined with respect to both the x- and y-axes. And the incident x-polarized and y-polarized waves will be

divided into four parts due to the interaction with the metallic layer B, e.g. x-polarized transmitted and reflected waves as well as y-polarized transmitted and reflected waves. In Fig. 5(a), the cross-polarized transmission coefficients T_{yx} have a maximum of 0.47 at 24 GHz, while co-polarized transmission coefficients T_{xx} have a magnitude greater than 0.32 in the whole frequency band.

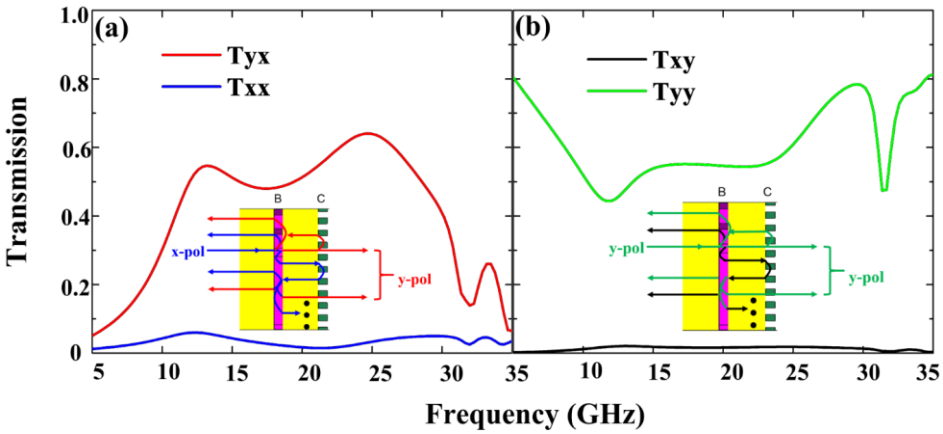

Fig. 6. Transmission coefficients of (a) x-polarized incident wave and (b) y-polarized incident wave: schematic graph of Fabry-Pérot-like mechanism model (side view of bi-layer BC).

Then, we add a y-polarization selective grating array (layer C) on the bottom layer. Thus, the structure will break the mirror symmetry in the wave propagating direction (-z), and making the curves of the transmission coefficients in Fig. 6(a) and (b) are different from each other. For the transmitted waves, the y-polarized waves can continually penetrate layer C, while the x-polarized waves are blocked and nearly reflected by layer C. So these parts of wave go back to the metallic layer B, where they are also divided into four parts. A portion of these waves will reflect with the x-polarization and y-polarization. For these reflected waves, the x-polarized components that are still blocked by layer C and reflected many times between the two metal layers. Eventually the many times reflecting waves nearly convert into the y-polarized waves, accounting for the conspicuous high transmission amplitude of T_{xx} compared to that of Fig. 5(a). Thus with the waves traveling back and forth between the two metallic layers, there is the Fabry-Pérot-like cavity between them, which results in a highly efficient polarization conversion [28]. For the y-polarized incident wave, due to the orientation of the grating, the co-polarized transmission coefficient has a larger magnitude than the cross-polarized transmission coefficient, as shown in Fig. 6(b).

Last, to further enhance the polarization conversion efficiency, we add an x-polarization selective grating (layer A) in front of the diamond metallic layer in an ABC stacks, and the Fabry-Pérot-like mechanism model is shown in Fig. 4. As previously mentioned, layer A is a sub-wavelength grating parallel to the y-axis, which is transparent to x-polarized waves while blocking the y-polarized components. So, most of the incident x-polarized waves can pass through it, while

the y-polarized waves will be near-thoroughly reflected when the linearly polarized waves illuminate layer A. Moreover, similar to the previous analysis, the last added layer A in the model of the bi-layer BC will block and reflect the traveling waves propagating in the z direction, which further contributes to the Fabry-Pérot effect and leads to a broad operating band and high magnitude property. These results can be seen from Fig. 2, in which the multi-layer stacks (ABC) realize a much higher polarization conversion (0.94) than the single-layer B (maximum 0.47) or bi-layer BC (maximum 0.7) in a broad operating band (10 GHz-30 GHz).

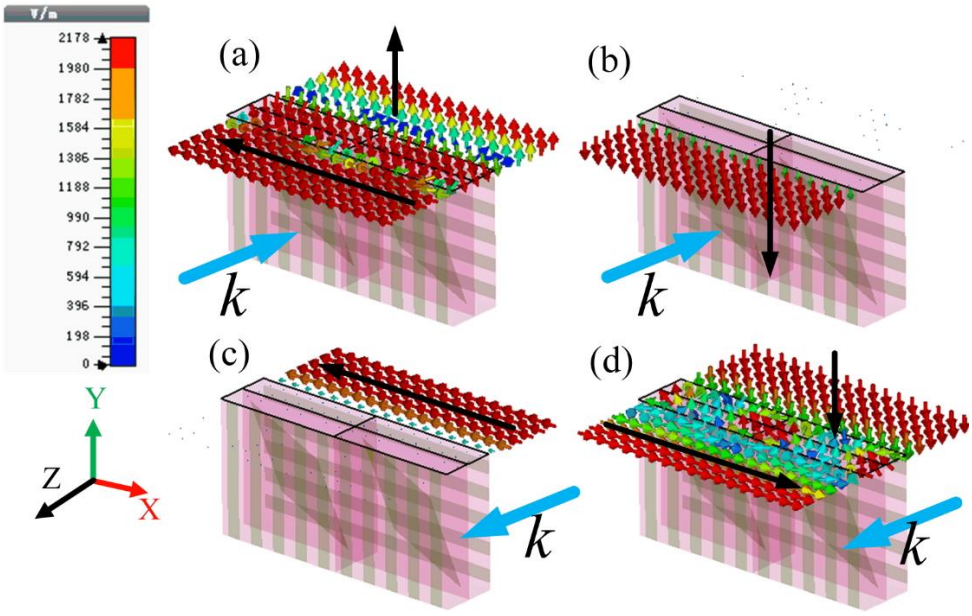

Fig. 7. Electric fields distribution of x-polarized and y-polarized incident waves at 14.5 GHz in -z direction (a), (b) and +z direction (c), (d).

In order to verify the AT effect of the proposed structure, we also use the CST Microwave Studio to simulate the electric fields distribution of the transmitted waves at 14.5 GHz when the linearly polarized waves illuminate the tri-layer structure both in the backward and forward direction. In Fig. 7 (a) and (b) we can clearly observe that the incident x-polarized waves can pass through the structure and convert into the y-polarized waves, while almost the entire y-polarized incident waves are blocked by the selective grating array and few of those convert into the x-polarized ones. In the Fig. 7 (c) and (d) only the y-polarized waves can pass through the structure and convert into the x-polarized ones, while almost the entire x-polarized incident waves are blocked by the x-direction grating array. We can find these results are in good agreement with the previous conclusions in Fig. 2. Then comparing both the Fig. 7(a) and (c) we can find that cross-polarized transmission coefficients T_{yx} in backward direction are different from those in forward direction. This is the so-called "Asymmetric transmission". Due to the distribution of the orthogonal selective grating on both top and bottom layer, there

are only a few of the undesirable transmitted waves on the received side. Similarly, in Fig. 7 (b) and (d) the cross-polarized transmission coefficients T_{xy} also exhibit the obvious asymmetric transmission effect between the both backward and forward direction. So we can conclude that our proposed the tri-layer chiral metasurface can achieve the asymmetric transmission effect from the 10 GHz to 30 GHz and have the excellent EM properties, such as broad operating band and high transmission magnitude.

4 Conclusion

In conclusion, we present a novel tri-layer chiral metasurface structure that consists of a grating array and diamond-shaped metallic strips. It can produce a significant asymmetric EM transmission phenomenon with a high cross-polarization transmission coefficient for linear polarization. Firstly, a notable characteristic of the proposed structure is its broad bandwidth in the microwave frequency range, which shows a remarkable advantage over the previous excellent structures. Then, the enhanced AT effect of the designed tri-layer structure can be attributed to the Fabry-Pérot-like mechanism effect. Moreover, our proposed structure is compactness both in the propagating direction and transverse directions ($\lambda/4.13 \times \lambda/4.13 \times \lambda/9.4$). With these excellent properties, the proposed structure is of great value for potential applications in areas such as the design of polarization conversion devices and nonreciprocal EM devices.

Acknowledgments

This work was financial supported by the National Natural Science Foundation of China under Contract No.61301120 and No.51377179 and 61571069, also partly by the Fundamental Research Funds for the Central Universities of CQU (CDJPY12160001).